Polarimetric Radar Variables in Snowfall at Ka- and W-Band Frequency Bands: A Comparative Analysis

SERGEY Y. MATROSOV[a,b]

[a] *Cooperative Institute for Research in Environmental Sciences, University of Colorado Boulder, Boulder, Colorado*
[b] *NOAA/Physical Sciences Laboratory, Boulder, Colorado*

(Manuscript received 17 August 2020, in final form 21 October 2020)

ABSTRACT: Dual-frequency millimeter-wavelength radar observations in snowfall are analyzed in order to evaluate differences in conventional polarimetric radar variables such as differential reflectivity (Z_{DR}) specific differential phase shift (K_{DP}) and linear depolarization ratio (LDR) at traditional cloud radar frequencies at Ka and W bands (~35 and ~94 GHz, correspondingly). Low radar beam elevation (~5°) measurements were performed at Oliktok Point, Alaska, with a scanning fully polarimetric radar operating in the horizontal–vertical polarization basis. This radar has the same gate spacing and very close beam widths at both frequencies, which largely alleviates uncertainties associated with spatial and temporal data matching. It is shown that observed Ka- and W-band Z_{DR} differences are, on average, less than about 0.5 dB and do not have a pronounced trend as a function of snowfall reflectivity. The observed Z_{DR} differences agree well with modeling results obtained using integration over nonspherical ice particle size distributions. For higher signal-to-noise ratios, K_{DP} data derived from differential phase measurements are approximately scaled as reciprocals of corresponding radar frequencies indicating that the influence of non-Rayleigh scattering effects on this variable is rather limited. This result is also in satisfactory agreement with data obtained by modeling using realistic particle size distributions. Observed Ka- and W-band LDR differences are strongly affected by the radar hardware system polarization "leak" and are generally less than 4 dB. Smaller differences are observed for higher depolarizations, where the polarization "leak" is less pronounced. Realistic assumptions about particle canting and the system polarization isolation lead to modeling results that satisfactorily agree with observational dual-frequency LDR data.

KEYWORDS: Snowfall; Ice particles; Radars/Radar observations

1. Introduction

Although millimeter-wavelength radars operating at Ka (~35 GHz)- and W (~94 GHz)-frequency bands were originally designed for cloud observations, they also proved to be a valuable tool for remote sensing of precipitating ice (e.g., Heymsfield et al. 2005; Matrosov et al. 2008). These radars are especially useful for measuring winter precipitation as signal attenuation by ice phase hydrometeors is significantly less than that by water drops. Most often, however, remote sensing (when conducted by cloud radars) is performed in a vertical beam mode and is based on relating nonpolarimetric radar measurables to winter precipitation characteristics.

The use of scanning polarimetric cloud radars provides additional opportunities to improve remote sensing of precipitation, since polarimetric radar variables contain more information about ice hydrometeor scatterers compared to simple reflectivity measurements (e.g., Ryzhkov and Zrnić 2019). While first scanning polarimetric Ka- and W-band cloud radars were able to measure only one polarimetric variable: depolarization ratio (e.g., Reinking et al. 2002; Matrosov et al. 2012), newer scanning cloud radars are sometimes fully polarimetric and provide additional measurements of differential reflectivity and differential phase, which are informative on cloud and precipitation microphysics. Most of the polarimetric remote sensing approaches, however, have been developed for lower frequencies (e.g., at S-band frequencies around 3 GHz) when scatterers are much smaller compared to radar wavelengths, so the Rayleigh scattering approximation, when backscatter is proportional to the fourth power of frequency (i.e., $\sim\nu^4$), is valid (e.g., Ryzhkov and Zrnić 2019).

The observational facilities of the U.S. Department of Energy (DOE) Atmospheric Radiation Measurement (ARM) Program at Alaska sites have been recently used for cloud and precipitation measurements with a second-generation scanning ARM cloud radar (SACR2) (e.g., Matrosov et al. 2017). This radar is an advanced fully polarimetric version of the original dual-frequency (Ka and W band) SACR (Kollias et al. 2020). It transmits horizontally (h) and vertically (v) polarized waves alternatively, which alleviates polarization cross-coupling effects. Radar pulses are transmitted in hhvvh blocks (N. Bharadwaj 2016, private communication). This radar also has closely matched beams (~0.3° beam widths) and pulse lengths (~60 m) for both frequencies, which essentially removes spatiotemporal uncertainties of matching radar data at two frequencies. Pulse repetition times between two consecutive h and v transmissions and the range gate spacings were ~0.19 ms and 30 m, correspondingly.

Non-Rayleigh scattering effects influence the equivalent radar reflectivity factor (Z_e) (hereafter reflectivity) in precipitating ice/snow particles especially at W band when Z_e is greater than about 0 dBZ (Matrosov et al. 2019). This results in W band reflectivities being smaller than those at Ka band and allows for inferring ice hydrometeor size and shape information from dual-frequency reflectivity measurements.

Corresponding author: Sergey Y. Matrosov, sergey.matrosov@noaa.gov

DOI: 10.1175/JTECH-D-20-0138.1

The magnitude of non-Rayleigh scattering effects on polarimetric radar variables, however, is not well known yet. The main objective of this study was to evaluate how Ka- and W-band polarimetric radar variables in ice clouds and snowfall are related and if there are significant trends in the Ka − W polarimetric variable differences associated with non-Rayleigh scattering, which could provide some potential to infer ice hydrometeor microphysical information using dual-frequency polarimetric radar measurements.

The conventional radar polarimetric variables, which are directly available from SACR2 measurements are differential reflectivity (Z_{DR}) which is defined as the logarithmic difference between copolar reflectivities on horizontal and vertical polarizations, differential phase shift between horizontally and vertically polarized received radar signals (Φ_{DP}) linear depolarization ratio (LDR), defined here as the logarithmic difference between reflectivities on cross-polar (i.e., vertical) and copolar (i.e., horizontal) polarizations when only horizontal polarization radar pulses are transmitted, and the copolar correlation coefficient (ρ_{hv}) between copolar horizontal and vertical polarization radar echo amplitudes.

2. Ka- and W-band polarimetric radar observation in snowfall

An example of SACR2 plan position indicator (PPI) measurements at Ka- and W-band frequencies during a 21 October 2016 Oliktok Point, Alaska (the radar site geographical location: 70.4958°N, 149.8868°W), observational event is shown in Fig. 1. Reflectivity (Z_e) data are hereafter referred to horizontal polarization measurements. The variability of polarimetric measurables during this ~10-h event was among the highest recorded and maximum reflectivities were reaching the highest levels (~23 dBZ at Ka band) observed in snowfall during the SACR2 Oliktok Point deployment (Matrosov et al. 2020). The W-band area coverage is generally smaller due to lower sensitivity of the W-band radar channel.

Temperatures in the atmospheric column remained below freezing throughout the entire period, which alleviated effects of potential attenuation and differential attenuation by the melting nonspherical hydrometeors which otherwise can be substantial, especially at W band (e.g., Sassen et al. 2007). Attenuation by supercooled cloud liquid is not expected to bias polarimetric variables as cloud droplets are practically spherical and they equally attenuate radar signals of both polarizations. Polarimetric variables are also immune to attenuation by the atmospheric gases (i.e., oxygen and water vapor) as gaseous attenuation affects horizontally and vertically polarized waves equally. Ice hydrometeors observed in situ during this event varied from small ice particles (~0.01–0.02 cm) to almost 1-cm-size snowflakes (Matrosov et al. 2017, 2020).

The event of 21 October 2016 was characterized by a wide variety of conditions ranging from weakly precipitating ice and mixed-phase clouds to heaver snowfall with precipitation rates of up to about 2 mm h^{-1} in terms of liquid water equivalent. Hydrometeor species observed near the ground and aloft included irregular shape particles including unrimed and rimed aggregates, as well as periods with pristine dendrites and hexagonal plates and mixtures of particles with different habits (Matrosov et al. 2020). Graupel particles were also observed during periods with high amounts of supercooled liquid water in the atmospheric column.

Generally, it is difficult to maintain smooth unattended radar operations at a such remote location as Oliktok Point. However, this event occurred during the tethered balloon sounding intensive operating period (IOP), and the radar was well conditioned for this IOP. The data in Fig. 1 indicate a large dynamic range in observed reflectivities and differential reflectivities as conditions near the radar site were changing from lightly precipitating ice clouds without measurable ground snow accumulations to relatively heavy snowfall. Differential reflectivities varied from near 0 dB to values in excess of 5 dB. Smaller Z_{DR} values were usually observed when quasi-spherical and larger particles were present. Higher Z_{DR} values were indicative of single pristine planar crystals such as dendrites and hexagonal plates (e.g., Matrosov 1991; Schrom and Kumjian 2018) dominating radar echoes. Overall, measurements conducted during this event were representative of a wide variety of snowfall conditions observed at the Oliktok Point site. All this makes the snowfall event of 21 October 2016 a convenient observational case to study differences in polarimetric radar variables at two cloud radar frequencies. The SACR2 data are available from the ARM data archive (Matthews et al. 2019a,b).

The industrial facilities at the Oliktok Point site present a significant amount of ground clutter and beam blockage for low radar beam elevation measurements. The data presented in Fig. 1 correspond to the 5° radar beam elevation angle and they were thresholded at a 5 dB signal-to-noise ratio (SNR). Even for such relatively high slant elevation angles, there are partial radar beam blockages in the azimuthal angle ranges of 110°–130°, 155°–175°, and 330°–345°. This blockage is mostly visible in reflectivity measurements. In addition to this, there is an area of strong ground clutter at around a 1.8 km range for the azimuthal angle interval between approximately 0° and 120°. This area is well visible in Ka-band Z_{DR}, K_{DP}, and (especially) LDR data. The radar data affected by the partial blockage and ground clutter were excluded from the further analysis.

The scanning mode copolar sensitivities of the radar were approximately −15 and −8 dBZ at a 5 km range for the 5 dB SNR level at the Ka- and W-band frequencies, correspondingly. Such a sensitivity disparity resulted in the fact that W-band power measurements were often noisier than those at Ka band, especially at longer distances. This is visible when comparing Ka- and W-band measurements in Fig. 1 as the area, where higher radar frequency data are reliably available, is much smaller than that for the lower frequency. Periodic vertical radar beam pointing measurements were used for correcting differential reflectivity data for offsets/biases at both frequencies. During the course of the event, the Z_{DR} corrections found from these vertical beam measurements were, on average, several tenths of 1 dB. Some variability in Z_{DR} corrections, however, was present, which suggest that small residual biases in differential reflectivity measurements could still be present.

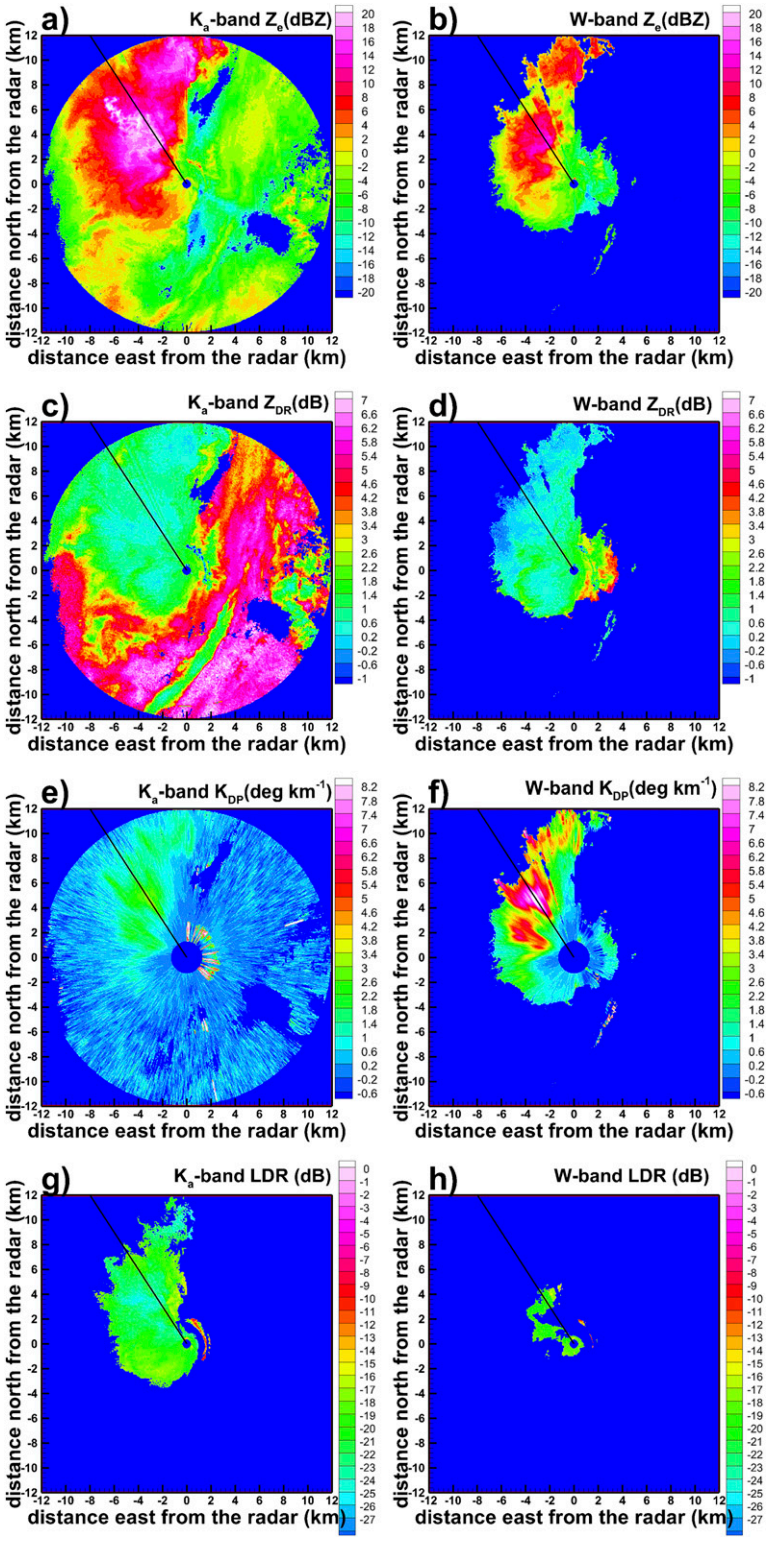

FIG. 1. The 5° elevation PPI data from SACR2 thresholded at 5 dB SNR at ~0438 UTC 21 Oct 2016. (a),(c),(e),(g) Ka band and (b),(d),(f),(h) W band. Horizontal polarization (a),(b) Z_e, (c),(d) Z_{DR}, (e),(f) K_{DP}, and (g),(h) LDR data. A 327° azimuth beam is shown by solid black lines. Data are averaged in 60 m × 60 m pixels.

For the entire observational event of 21 October 2016, Fig. 2 shows frequency scatterplots of Z_e(Ka) versus the differential reflectivity difference (ΔZ_{DR}) which is defined as Z_{DR}(Ka) − Z_{DR}(W). For low reflectivity values (e.g., ~−10 to −15 dBZ), scattering at both frequencies tends to be in the Rayleigh scattering regime (e.g., Matrosov et al. 2019), so differential reflectivity differences are expected to fluctuate around 0 dB as is the case for the data in Fig. 2. Interestingly, as reflectivity increases, ΔZ_{DR} values, on average, remain rather small (less than about 0.5 dB on average, though individual point differences can be as high as 2 dB or so). There are little (if any) robustly identifiable ΔZ_{DR}–Z_e(Ka) trends. Since reflectivity usually is well correlated with hydrometeor characteristic size such as a median volume size of particle populations (e.g., Matrosov and Heymsfield 2017), it might suggest that the non-Rayleigh scattering effects play a relatively little role in differential reflectivity values of ice hydrometeor populations at Ka- and W-band radar frequencies. For individual crystals, however, differences in Ka- and W-band differential reflectivities (as modeling shows) could be significant (Schrom and Kumjian 2018).

Attenuation effects might potentially reduce Z_e(Ka) and differential attenuation effects in ice might cause biases in ΔZ_{DR}. The severity of these effects is expected to increase with range. To evaluate their importance, Fig. 2b shows the data collected for the radar ranges $R \leq 6$ km as opposed to Fig. 2a where data are shown for $R \leq 12$ km. Comparing Figs. 2a and 2b indicates relatively little difference in the data scatter/trends, though some larger ΔZ_{DR} variability for higher reflectivities can be seen in Fig. 2a. Overall data in Figs. 2a and 2b suggest that attenuation/differential attenuation influence on Z_e(Ka)–ΔZ_{DR} correspondences for this observational event is rather small and can be neglected (at least, given several tenths of 1 dB uncertainties of differential reflectivity measurements).

Since Z_{DR}(Ka) generally increases as particles become more nonspherical, Z_{DR}(Ka)–ΔZ_{DR} correspondences can provide information on how non-Rayleigh scattering effects are influenced by particle nonsphericity. Figure 3 presents a frequency scatterplot for the Z_{DR} (Ka)–ΔZ_{DR} measurements. As can be seen from this figure, there is a slight (though not very distinct) tendency of ΔZ_{DR} increasing as Z_{DR} (Ka) becomes larger. However, even for higher observed values of Z_{DR} (Ka) (e.g., ~5 dB) an average ΔZ_{DR} remains smaller than about 1 dB, which is about 20% of differential reflectivity values (when expressed in the logarithmic scale).

Specific differential phase shift (K_{DP}) is not available from radar measurements directly, rather it is derived as half of the range derivative of differential phase (Φ_{DP}) which is a measured parameter; however, K_{DP} is a valuable polarimetric radar variable, which can improve radar-based retrievals of ice mass content and quantitative precipitation estimation (QPE) measurements in snowfall (Bukovčić et al. 2018). Values of K_{DP}, examples of which are shown in Fig. 1, were derived using the least squares method applied to filtered Φ_{DP} data (e.g., Matrosov 2010). The Φ_{DP} range interval used for K_{DP} calculations was 1.8 km, and an additional Φ_{DP} filtering using data thresholding based on the copolar correlation coefficient ($\rho_{hv} > 0.98$) was applied to reduce noise.

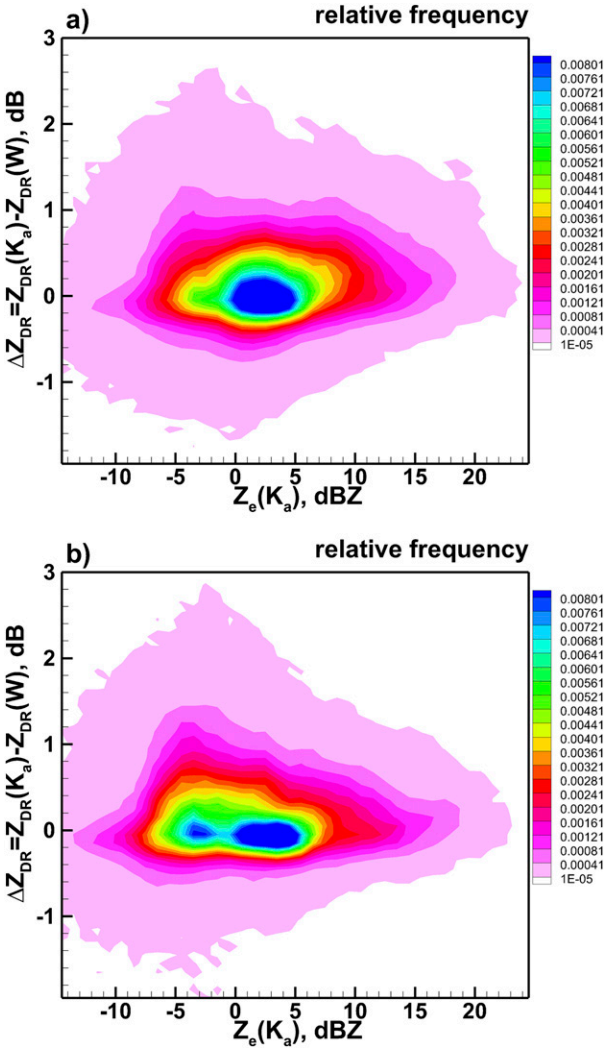

FIG. 2. Frequency scatterplots of observed Z_e(Ka) vs ΔZ_{DR} for ranges (a) $R \leq 12$ km and (b) $R \leq 6$ km.

In the Rayleigh scattering regime, K_{DP} values at two different radar frequencies, ν_1 and ν_2 are scaled as these frequencies (e.g., Bringi and Chandrasekar 2001):

$$K_{DP}(\nu_1)\,\nu_1^{-1} = K_{DP}(\nu_2)\,\nu_2^{-1}. \quad (1)$$

A scatterplot of observed SACR2 Ka-band reflectivity versus the frequency-scaled K_{DP} ratio defined as $[K_{DP}(W)K_{DP}^{-1}(Ka)]$ $[\nu^{-1}(W)\nu(Ka)]$ is shown in Fig. 4. K_{DP} is generally a noisier polarimetric variable compared to Z_{DR}, especially for smaller reflectivities and lower radar frequencies (e.g., Matrosov et al. 2006). To reduce noisiness, the data in Fig. 4 were additionally thresholded using a 20 dB SNR level at the W-band frequency measurements.

As seen from Fig. 4, the noisiness in the K_{DP} ratio gradually reduces as reflectivities becomes larger and most of the data points for Z_e(Ka) greater than about 10 dBZ are within 0.8 and 1.2. For lower reflectivities, the K_{DP} ratio data scatter is

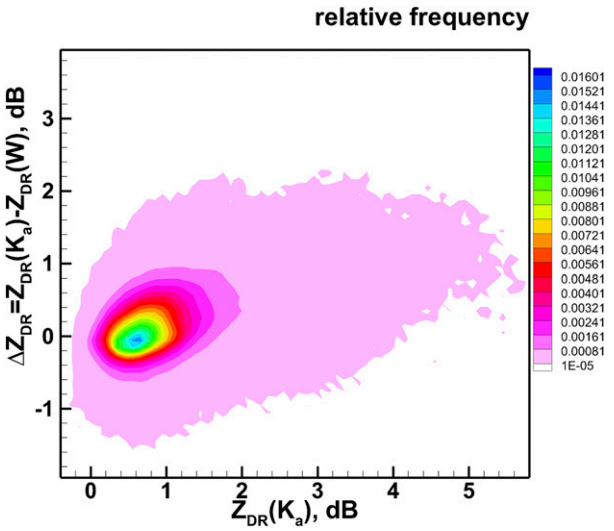

FIG. 3. Frequency scatterplots of observed Z_{DR}(Ka) vs ΔZ_{DR} for ranges $R \leq 12$ km.

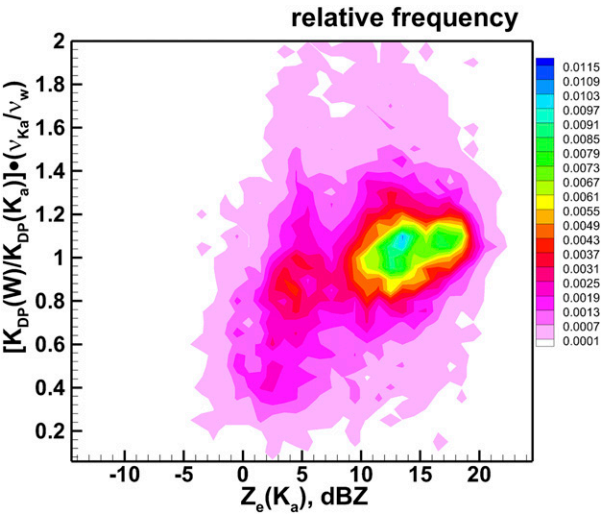

FIG. 4. Frequency scatterplots of the scaled ratio $[K_{DP}(W)/K_{DP}(Ka)]$ $[\nu(Ka)/\nu(W)]$ vs Z_e(Ka) for observational data at ranges $R \leq 12$ km.

significant. As seen from (1), for the Rayleigh type of scattering, the frequency-scaled K_{DP} ratio is expected to be 1. Given noisiness/uncertainties of specific differential phase calculations, the data in Fig. 4 indicate that for higher reflectivities/SNRs, non-Rayleigh scattering effects in K_{DP} are not very pronounced even for such high radar frequencies, as those used in the SACR2. This fact can potentially have a practical significance for snowfall QPE using scanning polarimetric cloud radars, as higher radar frequency K_{DP} values are larger in magnitude and thus they are generally less noisy (for a given SNR value) compared to those at lower radar frequencies. The K_{DP} ratio data did not exhibit much sensitivity as a function of observed Z_{DR} (Ka) (not shown).

An example of strong differential phase observed during heavier snowfall is shown in Fig. 5. The presented data correspond to the radar beam measurements in the azimuthal direction of 327° during a PPI scan shown in Fig. 1. W-band SNR values beyond the range of about 9 km are less than about 3 dB, so corresponding data are not shown. The mean two-way Φ_{DP} slopes between ranges $R = 4$ km and $R = 7$ km, where $\Phi_{DP}(R)$ at both frequencies exhibits approximately linear trends, are about 6.2° and 17.3° km^{-1} for the SACR2 Ka and W bands, respectively. The ratio of these slopes corresponds well to the ratio of the frequencies (i.e., 6.2° km^{-1}/17.3° km^{-1} $\approx$ 0.36 versus 35.29 GHz/93.93 GHz $\approx$ 0.37), so the frequency-scaled K_{DP} ratio is around 1. There is no evidence of a significant backscatter phase shift. Note that phase measurements are not affected by partial beam blockage and K_{DP} values generally correspond to the half of the two-way Φ_{DP} slopes. Differential reflectivity data at Ka and W bands in Fig. 5 approximately follow each other.

As seen from Figs. 1g and 1h, SACR2 LDRs in snowfall are generally very small. They are only available in the areas of higher SNR. This is due to the fact that the cross-polar radar echoes are usually 1.5 to 3 orders of magnitude weaker than copolar ones. For reliable LDR measurements, SNR thresholding needs to be performed using signals obtained in the cross-polar receiving channel. In addition to dependence on hydrometeor shape and bulk density, LDR values are also very sensitive to particle orientations, which presents a practical challenge for a quantitative interpretation of depolarization measurements conducted in the linear horizontal–vertical polarization basis.

Figure 6 shows a frequency scatterplot of the observed LDR(Ka) values versus the LDR(Ka)–LDR(W) difference. It should be mentioned that unlike for Z_{DR} and K_{DP} (in the alternate transmission mode) that are polarimetric variables describing copolar power and phase of radar signals, LDR values are strongly affected (especially small LDR values) by the radar hardware ''cross talk,'' which describes polarization ''leaks'' between horizontally and vertically polarized signals. This ''cross talk'' depends on the polarization isolation of horizontal and vertical polarization radar channels and is characterized by the minimum measurable linear depolarization ratio, LDR_{min}, which is observed when scatterers are spherical. Measurements in drizzle, whose drops are practically spherical, indicated that the SACR2 Ka-band LDR_{min} values were approximately −26 dB (Matrosov et al. 2017), while at W band they were only about −22 dB.

The dynamic range of observed LDR values is rather small (i.e., around 8 dB in Fig. 6). The data in Fig. 6 suggest that the absolute difference between Ka- and W-band LDR gradually decreases as LDR increases. For higher LDR values, this difference is less than about 1 dB. The difference for lower LDR values is around −4 dB, which is (as expected) close to the Ka–W-band LDR_{min} discrepancy. The regions of larger reflectivities usually are characterized by lower LDR (e.g., Fig. 1a vs Fig. 1g) as Z_e is often dominated by larger particles, which are generally less dense compared to smaller particles. For a given particle shape, LDR diminishes as density decreases.

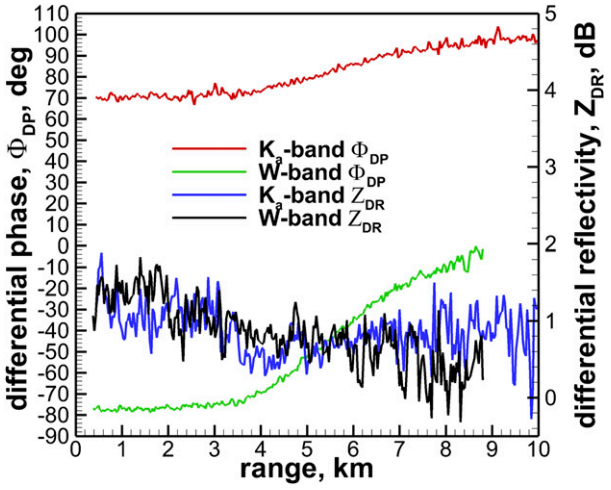

FIG. 5. SACR2 differential phase (left y axis) and differential reflectivity (right y axis) measurements along a 5° elevation–327° azimuth radar beam. The beam direction is shown by solid black lines in Fig. 1.

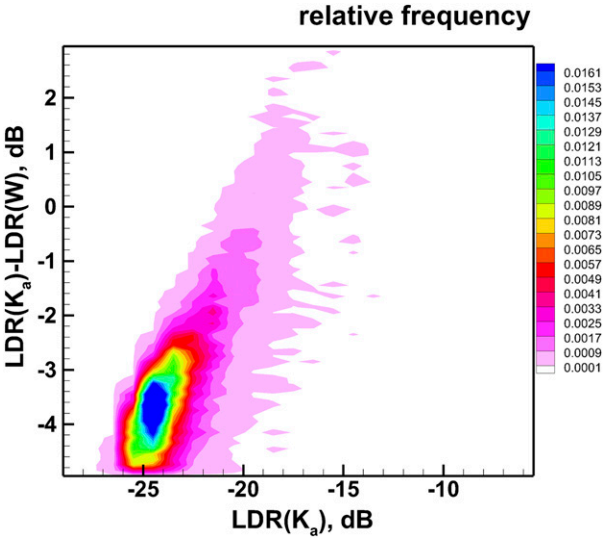

FIG. 6. Frequency scatterplots of observed LDR(Ka) vs LDR(Ka) − LDR(W) for ranges $R \leq 12$ km.

Copolar correlation (ρ_{hv}) values were estimated for the zero-lag time from one-lag measurements of consecutive h and v pulses (N. Bharadwaj 2016, private communication). Comparisons of collocated Ka- and W-band ρ_{hv} data indicated that ρ_{hv}(W) values were consistently smaller than ρ_{hv}(Ka) values (not shown). A noticeable mean difference between ρ_{hv}(Ka) and ρ_{hv}(W) of about 0.01 remained even if only the data with high SNR (>20 dB) and reflectivities less than −5 dBZ (i.e., where the Rayleigh scattering regime at both frequencies was expected) were considered. The reasons for that discrepancy are not well known yet. This issue requires a special consideration in future studies.

3. Modeling differences in Ka- and W-band radar variables

a. *Polarimetric radar variables*

Relatively small differences in Ka- and W-band Z_{DR}, LDR, and frequency-scaled K_{DP} values as obtained from the SACR2 measurements in precipitating ice/snow suggest that there is only a rather modest influence of non-Rayleigh scattering on these radar variables. This is in contrast to Ka–W-band differences in vertical Doppler velocities and dual-wavelength ratio (DWR) reflectivity differences, which could be significant (Matrosov 2011). One possible reason for smaller influence of non-Rayleigh scattering on polarimetric variables is that they are differential (rather than absolute) quantities representing differences/ratios of radar parameters at two orthogonal polarizations. In any case, it is instructive to conduct modeling of polarimetric radar variable differences/ratios to better understand the observational results.

A simple oblate spheroidal particle shape was assumed for modeling here. Under this assumption, a general particle shape is described by an aspect ratio parameter, which is defined as a ratio of particle minor-to-major dimensions. A spheroidal model is often used to represent nonspherical atmospheric hydrometeors (e.g., Bringi and Chandrasekar 2001; Ryzhkov and Zrnić 2019). An oblate rather than a prolate spheroidal shape was chosen here because the elevation angle dependencies of depolarization (i.e., when minimal depolarization values are observed near the zenith viewing direction with a general increase in depolarization when moving toward lower radar beam elevations) indicated the dominance of planar-type habits of precipitating ice hydrometeors (Matrosov et al. 2017).

Although a spheroidal shape has limitations for modeling particles with very low aspect ratios, such as pristine dendrites (e.g., Schrom and Kumjian 2018), it is still a practical assumption when modeling irregularly shaped ice hydrometeors, which often dominate radar returns and are the most common observed ice particle habit (e.g., Matrosov et al. 2017). Polarimetric radar variables are determined by backward (for Z_{DR} and LDR) and forward (for K_{DP}) amplitude scattering matrix elements. Equations for radar variables as functions of the matrix elements are given in many textbooks [e.g., Doviak and Zrnić 1993, their Eqs. (8.30) and (8.46)]. The T-matrix approach (e.g., Mishchenko and Travis 1994) was further used in this study for calculating elements of the scattering matrix.

Calculations were performed for an ensemble of ice hydrometeors by integrating scattering matrix elements over particle sizes, D, (expressed in terms of major particle dimensions) in the interval between 50 μm and 1 cm. It was assumed that the particle size distribution (PSD) was exponential:

$$N = N_0 \exp(-3.67 D D_{mv}^{-1}), \quad (2)$$

where D_{mv} is the median volume particle size. In situ hydrometeor sampling shows that exponential distributions are commonly observed in precipitating ice clouds and snowfalls (e.g., Matrosov and Heymsfield 2017). Note that PSD integrated reflectivity dual-wavelength ratios at cloud radar frequencies calculated using the T-matrix approach were

previously found to be in good agreement with the results from the self-similar Rayleigh–Gans technique (Matrosov et al. 2019) as applied to the vertically pointing beam geometry. This technique, in turn, was verified using the exact discrete dipole approximation (DDA) calculation method (Hogan and Westbrook 2014). The self-similar Rayleigh–Gans technique, however, is not well suited for calculating polarimetric radar variables at slant radar beam geometries.

The complex refractive index of ice hydrometeors, which is required for calculating scattering matrix elements under the T-matrix approach was computed using the Maxwell-Garnett rule (1904) for air–solid ice mixtures. The solid ice volume fraction, which is dependent on particle size, was determined based on particle bulk density defined as the ratio of the particle mass to its volume. It was further assumed that the particle mass–size relation (i.e., m–D relation) is described by a power law:

$$m = \alpha D^{\beta}. \tag{3}$$

The coefficients α and β in (3) were assumed to be 0.0046 and 2.1 (cgs units hereafter), correspondingly. These coefficients were adopted from the study of von Lerber et al. (2017), who showed that they adequately describe in situ observational results for unrimed and low-rimed snowfall conditions. For moderately rimed particles they found $\alpha = 0.0053$ and $\beta = 2.1$, which represents a relatively minor increase in α. These coefficient values are practically identical to the ones found in an earlier study by Heymsfield et al. (2013), who used in situ measurements with two-dimensional particle probes and ice mass bulk data utilizing a counterflow virtual impactor.

In model calculations of polarimetric variables, the $D_{\rm mv}$ parameter in (2) varied between 0.04 and 0.3 cm and the intercept parameter N_0 was chosen to be 0.08 $\rm cm^{-3}$. Although polarimetric radar variables (i.e., $Z_{\rm DR}$, LDR and the frequency-scaled $K_{\rm DP}$ ratio) do not depend on the intercept N_0, reflectivity values are proportional to it. Reflectivity values also change with changes in $D_{\rm mv}$. Such a choice of the exponential PSD, the m–D relation coefficients and the $D_{\rm mv}$ values provides a realistic range of observed Ka-band reflectivities (from ~ -15 to $\sim$22 dBZ). Besides, it results in an approximate power-law relation between ice water content (IWC) and Ka-band radar reflectivity: IWC (g $\rm m^{-3}$) $\approx 0.065\ Z_e^{0.68}$ ($\rm mm^6\,m^{-3}$), which is close to the one found from in situ PSDs (Matrosov and Heymsfield 2008) and within those inferred from multisensor retrievals (Matrosov 1997). Overall, it suggests that this choice of parameters/assumptions is reasonable to provide realistic model calculations of polarimetric radar variable differences/ratios for comparisons with observations.

For two assumptions of particle aspect ratios (i.e., AR = 0.3 and 0.8), Fig. 7a shows modeled differential reflectivity differences $\Delta Z_{\rm DR}$ and the frequency-scaled $K_{\rm DP}$ ratios as functions of Ka-band reflectivity. As seen from this figure, modeled $\Delta Z_{\rm DR}$ values remain relatively small for the entire range of reflectivity changes, even though some decreasing trend, when Z_e(Ka) is increasing, is present for particles with a higher degree of nonsphericity (i.e., AR = 0.3). It should be also noted that, as a result of the integration with respect to the PSD, there

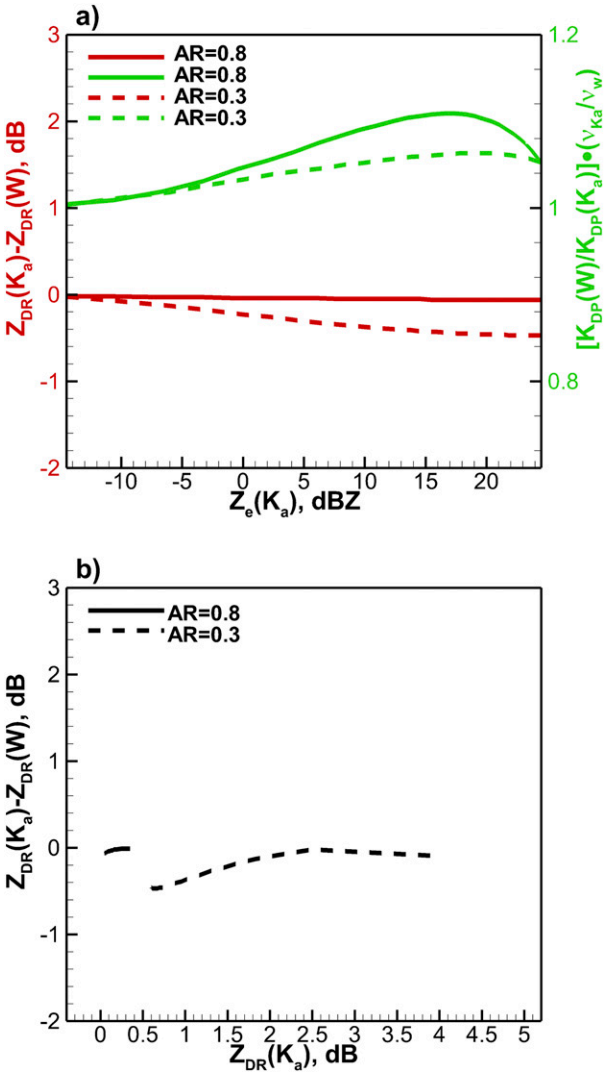

FIG. 7. Model calculations of (a) differential reflectivity difference (red, left y axis) and $K_{\rm DP}$ scaled ratio (green, right y axis) as a function of Ka-band reflectivity and (b) differential reflectivity difference as a function of differential reflectivity. Solid and dashed curves correspond to aspect ratios of 0.8 and 0.3, respectively. Radar beam elevation angle is 5°.

are no Mie scattering–like resonances in the modeled polarimetric variables even at W band, so the modeled $\Delta Z_{\rm DR}$–Z_e(Ka) correspondences are rather smooth. Given that several tenths of 1 dB uncertainties in differential reflectivity measurements are likely, the observations (Fig. 2) and model data agree, on average, reasonably well.

The model calculations of frequency-scaled $K_{\rm DP}$ ratios in Fig. 7a indicate some variability of this ratio with reflectivity, however, deviations of this ratio from 1 is, for the most part, less than about 10%. While the influence of particles' aspect ratio on modeled data exists, it is not very strong. Given uncertainties of deriving $K_{\rm DP}$ from differential phase measurements (and also modeling uncertainties), the agreement between observational data of the frequency-scaled $K_{\rm DP}$ ratios

(Fig. 4) and their model calculations is overall satisfactory (specifically for higher reflectivities, which generally correspond to larger SNRs).

Figure 7b shows modeled differential reflectivity differences ΔZ_{DR} as a function of Ka-band differential reflectivity. Note that Z_{DR} values change even for a fixed AR value due to changes in particle bulk density which is decreasing with an increase in particle characteristic size. While for more spherical particles (i.e., AR = 0.8), ΔZ_{DR} and Z_{DR}(Ka) are around a 0 dB value, there is a weak increasing trend of ΔZ_{DR} with Z_{DR}(Ka) as size dependent bulk density changes for hydrometeors with a higher degree of nonsphericity. Such a trend is also evident from observations (Fig. 3). Although modeled and observational data are mutually biased by a few tenths of 1dB in a mean sense, calculated and measured ΔZ_{DR} values overall remain rather small in the absolute sense.

The ΔZ_{DR} and K_{DP} data in Fig. 7 were calculated assuming that particles are oriented with their major dimensions in the horizontal plane, so the particle canting angle is zero. Such preferable particle orientation is dictated by air dynamic forcing. Particles, however, usually flutter around the horizontal orientation and the amount of this flutter is approximately in an interval between 2° and 23° (e.g., Melnikov 2017). Accounting for a particle flutter of this magnitude does not significantly change the results shown in Fig. 7. This is because particle orientation fluttering affects Z_{DR} and K_{DP} at both frequencies similarly. The fact that modeled ΔZ_{DR} values are small for different assumptions of particle aspect ratios suggests that these values remain small for mixtures of particles of different shapes.

The Z_{DR} and K_{DP} are important polarimetric radar variables and they are often used quantitatively in many practical applications ranging from studies of microphysical processes in clouds and precipitation to QPE. Linear depolarization ratios are used not that often. Unlike the frequency-scaled K_{DP} ratio and ΔZ_{DR}, LDR is very sensitive to particle flutter. Besides, LDR can reliably be measured only when the cross-polarization echo SNR is high enough. In part, due to these reasons, LDR often is used only qualitatively. It is instructive, however, to compare modeled LDR characteristics with the observed data presented in Fig. 6.

For the same range of linear depolarization ratio values as in Figs. 6, Fig. 8 depicts modeled differences in Ka- and W-band LDR values as a function of LDR(Ka). The presented data correspond to several assumptions for the mean absolute value of particle canting angle α, which characterizes hydrometeor flutter around the orientation with major dimensions in the horizontal plane. The radar hardware system polarization ''cross talk'' was accounted for. The modeled data are shown for $LDR_{min}(Ka) = -26$ dB and $LDR_{min}(W) = -22$ dB (as mentioned previously) and also, to illustrate the hardware influences, for $LDR_{min}(Ka) = -25$ dB and $LDR_{min}(W) = -21$ dB. Modeling was performed for several values of α (~10°–20°) using the same PSD assumptions as for Z_{DR} and K_{DP} calculations. Details of accounting for the radar system polarization ''cross talk'' are given in Matrosov (2015).

Comparing Figs. 6 and 8 indicates that there is a general correspondence between modeled data and observations.

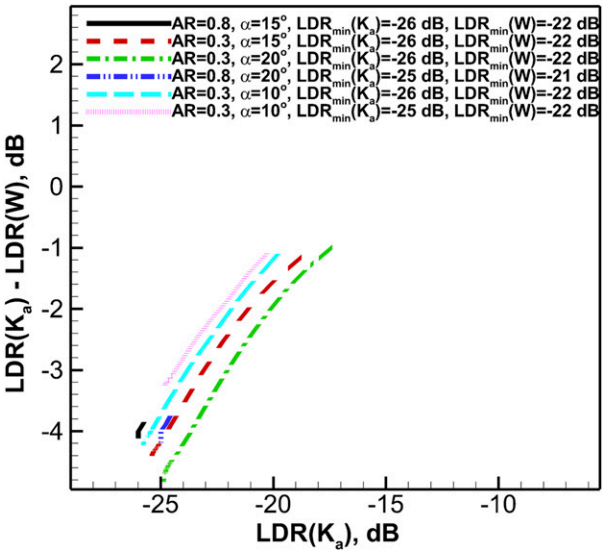

FIG. 8. Model calculations of LDR(Ka) − LDR(W) differences as a functions of Ka-band LDR. Radar beam elevation angle is 5°.

More spherical ice particles with aspect ratios of 0.8 produce lower LDR and larger absolute values of Ka–W-band LDR differences for the entire range of model parameters. Hydrometeors with a greater degree of nonsphericity (i.e., AR = 0.3) exhibit a larger dynamic range of depolarization changes. Lower LDR values are associated with larger reflectivities and thus larger particle characteristic sizes. Larger particles are ''optically softer'' (i.e., less dense) than smaller ones thus they produce lower levels of radar signal depolarization. Compared to larger particles, smaller (and denser) particles with the same aspect ratios and orientation produce larger LDR values.

b. *Elevation angle dependences of dual-wavelength ratios*

Presented observational and modeled data indicate that for ice hydrometeor populations, the non-Rayleigh scattering effects at millimeter-wavelength cloud radar frequencies are not very strong for common polarimetric variables such as Z_{DR} and K_{DP}. This is in contrast with magnitudes of these effects when considering the dual-wavelength ratio (DWR), which is defined as the logarithmic difference between reflectivities at two frequencies. Due to these effects, DWR values in precipitating ice clouds and snowfall observed by the SACR2 vary significantly with reflectivity (and with characteristic particle size) and could exceed 10 dB or so (e.g., Matrosov et al. 2019). At vertical incidence, DWR also significantly depends on particles' degree of nonsphericity with more spherical particles producing higher DWR values compared to hydrometeors with smaller AR values for similar reflectivities and characteristic sizes. As a result, Z_e(Ka)–Ka/W-band DWR correspondences can be used to segregate between pristine crystal and aggregate particle populations (Matrosov et al. 2019).

For low radar elevation angles and particles oriented predominantly with larger dimensions in the horizontal plane, DWR variability due to hydrometeor aspect ratio changes is

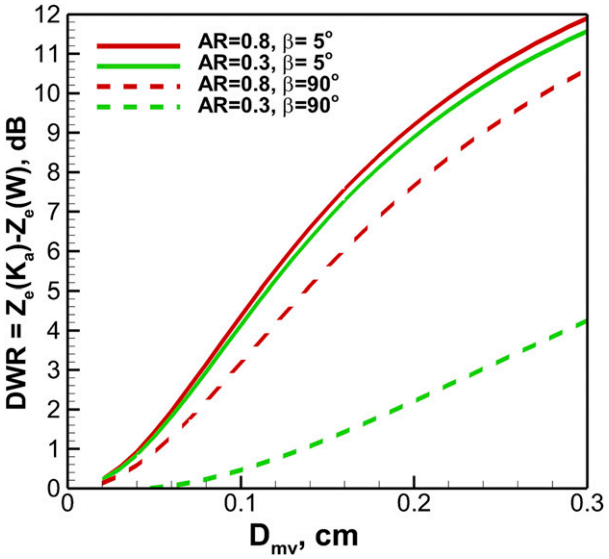

FIG. 9. Ka–W-band dual wavelength ratio as a function of median volume particle size for two assumptions of particle aspect ratios (AR = 0.3 and AR = 0.8) and two radar beam elevation angles ($\beta = 5°$ and $\beta = 90°$).

largely diminished as compared to vertical viewing. To illustrate this point, Fig. 9 shows model calculations of DWR as a function of median volume particle size D_{mv} for vertical and slant viewing directions. It can be seen from this figure that DWR values are maximized for low elevation angle radar pointing and the DWR variability due to particle shapes is largely reduced for such pointing. This fact can have an important practical implication for applying multifrequency radar techniques as it suggests that the DWR radar observations at lower beam elevations are preferable compared to vertical viewing for the purpose of inferring characteristic particle sizes.

4. Conclusions

Matched in space and time low-elevation angle dual-frequency cloud radar measurements in snowfall were used to evaluate correspondences between horizontal–vertical basis polarimetric variables at Ka- and W-band frequencies. The observational dataset was collected at an Arctic location by the advanced DOE ARM dual-wavelength fully polarimetric scanning radar. The event analyzed in this study was representative of precipitating ice/snowfall conditions observed during the radar deployment at Oliktok Point, Alaska. Ice hydrometeors of various habits were present during this event. Observed conventional and polarimetric radar variables varied in wide dynamic ranges.

The measurements revealed that Ka–W-band differential reflectivity differences (ΔZ_{DR}) remained relatively small for the entire range of observed reflectivities, which indicates that the influence of non-Rayleigh scattering effects on differential reflectivity of particle populations at cloud radar frequencies is rather small. Although typical ΔZ_{DR} fluctuations around the 0 dB value were mostly less than several tenths of 1 dB, differences of around 1 dB were not uncommon. The differential reflectivity measurements at each frequency were calibrated using vertical radar beam measurements to minimize Z_{DR} measurement biases/offsets.

The results of theoretical modeling of ΔZ_{DR} values using the T-matrix approach were in general agreement with observations. Even though, the model calculations performed for different assumptions of the hydrometeor degree of nonsphericity (as expressed by the particle aspect ratios AR = 0.3 and 0.8), suggested possibility of some weak ΔZ_{DR} trends with increasing reflectivities for particles with higher degrees of nonsphericity, absolute values of theoretical ΔZ_{DR} remained generally small and comparable with uncertainties of differential reflectivity measurements. ΔZ_{DR} measurement errors and model uncertainties could have contributed to small biases between theoretical and observed differential reflectivity differences. It can be also hypothesized that integration over particle size distributions leads to reducing non-Rayleigh scattering effects, which otherwise might be present for individual hydrometeor scatterers, especially at W band.

Specific differential phase shift (K_{DP}) estimates from Φ_{DP} measurements are usually more reliable for higher reflectivities and larger SNRs. For reflectivities greater than about 10 dBZ, the frequency-scaled W–Ka-band K_{DP} ratios were generally within 0.8 and 1.2 thus deviating relatively little from 1, which is the value for the Rayleigh type scattering scaling for this radar variable. Such a variability in the observationally derived K_{DP} ratios is, in part, due to a natural noisiness of measured differential phase data.

While theoretical modeling of frequency-scaled K_{DP} ratios indicated some variability with reflectivity, this variability generally did not exceed about 10% from the unity value. Overall, the agreement between observationally derived and modeled frequency-scaled K_{DP} ratios was satisfactory for reflectivities greater than about 10 dBZ. Since K_{DP} is a noisy polarimetric radar variable, the observed frequency scaling of specific differential phase has an important practical implication as larger (and hence more reliably derived) K_{DP} values at higher radar frequencies might be advantageous for some applications (e.g., snowfall QPE at close radar ranges).

Observed Ka–W-band linear depolarization ratio differences generally varied between about −5 and 1 dB. Smaller (larger) absolute value LDR differences were generally observed for higher (lower) Ka-band LDR values. This observational result was generally consistent with differing radar system polarimetric ''cross talk'' leak characteristics of the SACR2 Ka- and W-band channels. Model calculations were able to approximately replicate the LDR observational results when realistic assumptions about hydrometeor canting were made.

Insignificant dual-wavelength effects on differential reflectivity and the dominance of polarimetric ''cross talk'' effects on linear depolarization ratio differences might make the potential use of dual-frequency polarimetric measurements utilizing

ΔZ_{DR} and LDR differences not very promising for the purpose of ice hydrometeor microphysical retrievals. Relatively small ΔZ_{DR} values and the approximate frequency scaling of K_{DP} are in contrast with significant non-Rayleigh scattering influences on Ka–W-band reflectivity DWR. DWRs previously observed using the SACR2 measurements could be as high 10 dB depending on particle characteristic size and shape. For hydrometeors with preferable horizontal orientation, the particle shape influence on DWR, however, is expected to be much weaker for slant radar viewing angles as compared to measurements with zenith/nadir radar beam pointing.

Acknowledgments. This research was funded by the U.S. Department of Energy's Atmospheric Systems Research (ASR) program (Grant DE-SC0013306) and the National Science Foundation (Grant AGS 1841260).

REFERENCES

Bringi, V. N., and V. Chandrasekar, 2001: *Polarimetric Doppler Weather Radar*. Cambridge University Press, 636 pp.

Bukovčić, P., A. Ryzhkov, D. Zrnić, and G. Zhang, 2018: Polarimetric radar relations for quantification of snow based on disdrometer data. *J. Appl. Meteor. Climatol.*, **57**, 103–120, https://doi.org/10.1175/JAMC-D-17-0090.1.

Doviak, R., and D. Zrnić, 1993: *Doppler Radar and Weather Observations*. Academic Press, 562 pp.

Heymsfield, A. J., Z. Wang, and S. Y. Matrosov, 2005: Improved radar ice water content retrieval algorithms using coincident microphysical and radar measurements. *J. Appl. Meteor.*, **44**, 1391–1412, https://doi.org/10.1175/JAM2282.1.

——, C. Schmitt, and A. Bansemer, 2013: Ice cloud particle size distributions and pressure-dependent terminal velocities from in situ observations at temperatures from 0° to −86°C. *J. Atmos. Sci.*, **70**, 4123–4154, https://doi.org/10.1175/JAS-D-12-0124.1.

Hogan, R. J., and C. D. Westbrook, 2014: Equation for the microwave backscatter cross section of aggregate snowflakes using the self-similar Rayleigh–Gans approximation. *J. Atmos. Sci.*, **71**, 3292–3301, https://doi.org/10.1175/JAS-D-13-0347.1.

Kollias, P., and Coauthors, 2020: The ARM radar network: At the leading-edge of cloud and precipitation observations. *Bull. Amer. Meteor. Soc.*, **101**, E588–E607, https://doi.org/10.1175/BAMS-D-18-0288.1.

Matrosov, S. Y., 1991: Theoretical study of radar polarization parameters obtained from cirrus clouds. *J. Atmos. Sci.*, **48**, 1062–1070, https://doi.org/10.1175/1520-0469(1991)048<1062:TSORPP>2.0.CO;2.

——, 1997: Variability of microphysical parameters in high-altitude ice clouds: Results of the remote sensing method. *J. Appl. Meteor.*, **36**, 633–648, https://doi.org/10.1175/1520-0450-36.6.633.

——, 2010: Evaluating polarimetric X-band radar rainfall estimators during HMT. *J. Atmos. Oceanic Technol.*, **27**, 122–134, https://doi.org/10.1175/2009JTECHA1318.1.

——, 2011: Feasibility of using radar differential Doppler velocity and dual-frequency ratio for sizing particles in thick ice clouds. *J. Geophys. Res.*, **116**, D17202, https://doi.org/10.1029/2011JD015857.

——, 2015: Evaluations of the spheroidal particle model for describing cloud radar depolarization ratios of ice hydrometeors. *J. Atmos. Oceanic Technol.*, **32**, 865–879, https://doi.org/10.1175/JTECH-D-14-00115.1.

——, and A. J. Heymsfield, 2008: Estimating ice content and extinction in precipitating cloud systems from CloudSat radar measurements. *J. Geophys. Res.*, **113**, D00A05, https://doi.org/10.1029/2007JD009633.

——, and ——, 2017: Empirical relations between size parameters of ice hydrometeor populations and radar reflectivity. *J. Appl. Meteor. Climatol.*, **56**, 2479–2488, https://doi.org/10.1175/JAMC-D-17-0076.1.

——, R. Cifelli, P. C. Kennedy, S. W. Nesbitt, S. A. Rutledge, V. N. Bringi, and B. E. Martner, 2006: A comparative study of rainfall retrievals based on specific differential phase shifts at X- and S-band radar frequencies. *J. Atmos. Oceanic Technol.*, **23**, 952–963, https://doi.org/10.1175/JTECH1887.1.

——, M. D. Shupe, and I. V. Djalalova, 2008: Snowfall retrievals using millimeter-wavelength cloud radars. *J. Appl. Meteor. Climatol.*, **47**, 769–777, https://doi.org/10.1175/2007JAMC1768.1.

——, G. G. Mace, R. Marchand, M. D. Shupe, A. G. Hallar, and I. B. McCubbin, 2012: Observations of Ice crystal habits with a scanning polarimetric W-band radar at slant linear depolarization ratio mode. *J. Atmos. Oceanic Technol.*, **29**, 989–1008, https://doi.org/10.1175/JTECH-D-11-00131.1.

——, C. G. Schmitt, M. Maahn, and G. de Boer, 2017: Atmospheric ice particle shape estimates from polarimetric radar measurements and in situ observations. *J. Atmos. Oceanic Technol.*, **34**, 2569–2587, https://doi.org/10.1175/JTECH-D-17-0111.1.

——, M. Maahn, and G. de Boer, 2019: Observational and modeling study of ice hydrometeor radar dual-wavelength ratios. *J. Appl. Meteor. Climatol.*, **58**, 2005–2017, https://doi.org/10.1175/JAMC-D-19-0018.1.

——, A. V. Ryzhkov, M. Maahn, and G. de Boer, 2020: Hydrometeor shape variability in snowfall as retrieved from polarimetric radar measurements. *J. Appl. Meteor. Climatol.*, **59**, 1503–1517, https://doi.org/10.1175/JAMC-D-20-0052.1.

Matthews, A., B. Isom, D. Nelson, I. Lindenmaier, J. Hardin, K. Johnson, and N. Bharadwaj, 2019a: Ka-band scanning ARM Cloud Radar (KASACRCFRPPIVH), ARM Mobile Facility (OLI) Oliktok Point, Alaska; AMF3 (M1). ARM Data Center, accessed 1 October 2019, https://doi.org/10.5439/1224837.

——, ——, ——, ——, ——, ——, and ——, 2019b: W-band scanning ARM Cloud Radar (WSACRCFRPPIVH), ARM Mobile Facility (OLI) Oliktok Point, Alaska; AMF3 (M1). ARM Data Center, accessed 1 October 2019, https://doi.org/10.5439/1224848.

Maxwell-Garnet, J. C., 1904: Colours in metal glasses and in metallic films. *Philos. Trans. Roy. Soc. London*, **203A**, 359–371, https://doi.org/10.1098/rsta.1904.0024.

Melnikov, V., 2017: Parameters of cloud ice particles retrieved from radar data. *J. Atmos. Oceanic Technol.*, **34**, 717–728, https://doi.org/10.1175/JTECH-D-16-0123.1.

Mishchenko, M. I., and L. D. Travis, 1994: T-matrix computations of light scattering by larger spheroidal particles. *Opt. Commun.*, **109**, 16–21, https://doi.org/10.1016/0030-4018(94)90731-5.

Reinking, R. F., S. Y. Matrosov, R. A. Kropfli, and B. W. Bartram, 2002: Evaluation of a 45° slant quasi-linear radar polarization for distinguishing drizzle droplets, pristine ice crystals, and less regular ice particles. *J. Atmos. Oceanic Technol.*, **19**, 296–321, https://doi.org/10.1175/1520-0426-19.3.296.

Ryzhkov, A. V., and D. S. Zrnić, 2019: *Radar Polarimetry for Weather Observations*. Springer, 486 pp.

Sassen, K., S. Matrosov, and J. Campbell, 2007: CloudSat spaceborne 94 GHz radar bright band in the melting layer: An attenuation driven upside-down lidar analog. *Geophys. Res. Lett.*, **34**, L16818, https://doi.org/10.1029/2007GL030291.

Schrom, R. S., and M. R. Kumjian, 2018: Bulk density representations of branched planar ice crystals: Errors in the polarimetric radar variables. *J. Appl. Meteor. Climatol.*, **57**, 333–346, https://doi.org/10.1175/JAMC-D-17-0114.1.

von Lerber, A., D. Moisseev, L. F. Bliven, W. Petersen, A. Harri, and V. Chandrasekar, 2017: Microphysical properties of snow and their link to Z_e–S relations during BAECC 2014. *J. Appl. Meteor. Climatol.*, **56**, 1561–1582, https://doi.org/10.1175/JAMC-D-16-0379.1.